Plasmonics: nonlinear optics, negative phase, and transformable transparency

Popov, Alexander, Myslivets, Sergey, Shalaev, Vladimir

Alexander K. Popov, Sergey A. Myslivets, Vladimir M. Shalaev, "Plasmonics: nonlinear optics, negative phase, and transformable transparency," Proc. SPIE 7395, Plasmonics: Nanoimaging, Nanofabrication, and their Applications V, 73950Z (2 September 2009); doi: 10.1117/12.824836

SPIE.

Event: SPIE NanoScience + Engineering, 2009, San Diego, California, United States

Invited Paper

Plasmonics: nonlinear optics, negative phase and transformable transparency

Alexander K. Popov[a], Sergey A. Myslivets[b] and Vladimir M. Shalaev[c]

[a]University of Wisconsin-Stevens Point, 812 Kensington Rd. Neenah, WI 54956, USA;
[b]Siberian Federal University and Institute of Physics of Russian Academy of Sciences, 660036 Krasnoyarsk, Russian Federation;
[c]Birck Nanotechnology Center and School of Electrical and Computer Engineering, Purdue University, West Lafayette, IN 47907, USA

ABSTRACT

The feasibilities and specific features of coherent nonlinear-optical energy transfer from control fields to a negative-phase signal are studied, and they are found to stem from the backwardness of electromagnetic waves inherent to negative-index metamaterials. Plasmonic metamaterials that possess negative group velocity for light waves promise a revolutionary breakthrough in nanophotonics. However, strong absorption inherent to such metal-dielectric nanocomposites imposes severe limitations on the majority of such applications. Herein we show the feasibility and discuss different nonlinear-optical techniques of compensating such losses, producing transparency, amplification and even generation of negative-phase light waves in originally strongly absorbing microscopic samples of plasmonic metal-dielectric nanostructured composites.

Keywords: Negative-index metamaterials, backward electromagnetic waves, optical parametric amplification, quantum control.

1. INTRODUCTION

Optical negative-index (NI) metamaterials (NIMs) form a novel class of artificial electromagnetic media that promises revolutionary breakthroughs in photonics (see for example[1]). Unlike ordinary positive-index (PI) materials (PIMs), the energy flow and wave vector (phase velocity) are counter-directed in NIMs, which determines their extraordinary linear and nonlinear optical (NLO) properties. Strong absorption is fundamentally inherent to plasmonic NIMs, which presents a severe detrimental factor toward their applications. Significant progress has been achieved recently in the design of bulk, multilayered, negative-index, plasmonic slabs.[2–5] The majority of NIMs realized to date consist of metal-dielectric nanostructures that have highly controllable magnetic and dielectric responses. The problem, however, is that these structures have losses that are difficult to avoid, especially in the visible range of frequencies. Irrespective of their origin, losses constitute a major hurdle to the practical realization of the unique optical applications of these structures. Therefore, developing efficient loss-compensating techniques is of a paramount importance. So far, the most common approach to compensating losses in NIMs is associated with the possibility of embedding amplifying centers in the host matrix.[1] The amplification is supposed to be provided through a population inversion between the energy levels of the embedded centers. Herein, we investigate several alternative options based on coherent, NLO energy transfer from the control optical field(s) to the negative-phase signal field through optical parametric amplification (OPA). Nonlinear optical responses in NIMs remain so far a less-developed branch of optics. On a fundamental level, the NLO responses of nanostructured metamaterials are not completely understood or characterized and cannot be predicted effectively to date. Nevertheless, it is well established that local-field enhanced nonlinearities can be attributed to plasmonic nanostructures, and some rough estimates of their magnitude can be obtained. The feasibility of crafting NIMs with strong NLO responses in the optical wavelength range has been experimentally demonstrated.[6,7] The extraordinary NLO properties of propagation processes in NIMs, such as second-harmonic generation, three-wave

Send correspondence to:
Alexander Popov: E-mail: apopov@uwsp.edu,
Vladimir Shalaev: E-mail: shalaev@purdue.edu, Telephone: +1(765) 494-9855

Plasmonics: Nanoimaging, Nanofabrication, and their Applications V,
edited by Satoshi Kawata, Vladimir M. Shalaev, Din Ping Tsai, Proc. of SPIE Vol. 7395,
73950Z · © 2009 SPIE · CCC code: 0277-786X/09/$18 · doi: 10.1117/12.824836

mixing (TWM) and four-wave mixing (FWM) OPA have been predicted and are in drastic contrast with their counterparts in natural materials.[8–18] Striking changes in the properties of nonlinear pulse propagation and temporal solitons,[19] spatial solitons in systems with bistability,[20–22] gap solitons,[23] and optical bistability in layered structures including NIMs[24,25] were revealed. A review of some of the corresponding theoretical approaches is given in.[26] Frequency-degenerate multi-wave mixing and self-oscillation of counter-propagating waves in ordinary materials have been extensively studied because of their easily achievable phase matching. Phase matching for three-wave mixing (TWM) and four-wave mixing (FWM) of contra-propagating waves that are far from degeneracy seems impossible in ordinary materials and presents a technical challenge in the metamaterials. This actually became possible only recently due to the advances in nanotechnology.[27–29] The possibility of TWM with mirrorless self-oscillation from two co-propagating waves with nearly degenerate frequencies that fall within an anomalous dispersion frequency domain and gives rise to generation of a far-infrared, difference-frequency, counter-propagating wave in an anisotropic crystal was proposed in[27] (and references therein) more than 40 years ago (see also[30]). However, far-infrared radiation is typically strongly absorbed in crystals, which presents a strong detrimental factor. For the first time, a TWM backward-wave (BW) mirrorless optical parametrical oscillator (BWMOPO) with all three significantly different optical wavelengths was recently realized.[29] Phase-matching of counter-propagating waves has been achieved in a submicrometer, periodically poled, NLO crystal, which has become possible owing to recent advances in nanotechnology. Both in the proposal[27] and in the experiment,[29] *the opposite orientation of wave vectors* was required for mirrorless oscillations due to the fact that a PI crystal was used in the implementation. As outlined, a major technical problem in creating BWMOPO stems from the requirement of phase matching with the opposite orientation of wave vectors in PIMs.

Herein, we show the feasibility of creating distributed feedback and BWMOPO where *an antiparallel orientation of wave vectors of the coupled waves is no longer required*. Thus BWMOPO at appreciably different frequencies becomes possible while all the wave vectors of the coupled waves remain co-directed. Such an opportunity makes phase matching much easier and is offered by the backwardness of electromagnetic waves, which is natural to NIMs. Consequently, we propose and describe possible methods of compensating the strong losses inherent in NIMs through OPA of backward waves. The accompanying processes that may either assist or alternatively prevent such compensation are discussed. Ultimately the possibilities of producing a robust, all-optically tailored transparency, amplification and even mirrorless optical parametric oscillation in originally strongly absorbing bulk microscopic NI samples of plasmonic metal-dielectric nanostructured composites are shown and confirmed through numerical simulations. Two options are discussed. One is an OPA that implements nonlinearities attributed to the building blocks of the NIMs.[6] The other option, a FWM sheme,[14] proposes independent engineering of a $\chi^{(3)}$ nonlinearity through embedded, resonant, NLO centers. In the vicinity of the resonances, $\chi^{(3)}$ is exceptionally strong. In addition, the optical properties of the composite can be tailored by means of quantum control. It is shown that the outcomes are strongly dependent on the relaxation properties of the coupled optical transitions and on the specific coupling schemes. A comparative analysis of several such schemes is given.

The paper is organized as follows. Section 2 describes the basic principles and extraordinary properties of coherent energy transfer between the ordinary and backward-traveling electromagnetic waves as compared to OPA in ordinary, PI materials. In Section 3 we discuss the dependence and output values of the energy distribution of the negative-phase signal and the ordinary idler across the NI slab on the ratio of their absorption indices and on the phase-mismatch. Here, control (fundamental) fields are assumed to be uniform across the slab, and the local linear and nonlinear parameters are assumed to be independent of the intensities of the control fields. The conclusions are valid for both TWM and FWM. The induced transparency exhibits a resonance behavior as a function of the control field intensity and the NIM slab thickness due to the backwardness of the light waves in NIMs. Usually, the resonances are narrow, especially if the parametric process is assisted by amplification of the idler due to Raman or population-inversion gain. The sample remains opaque anywhere beyond the resonance magnitudes of the control field and the resonance thickness of the sample. Counterintuitively, we show that transparency becomes achievable within a broad range of these parameters if the absorption for the idler exceeds that for the signal. We also show that, in the above indicated case, the transparency of a NIM slab becomes much more robust against the phase mismatch. Based on these outcomes, we propose and investigate the option of independent engineering of the NI and FWM nonlinear response in Section 4. Here, we consider a doped metamaterial, where the signal appears in the vicinity of the transition between the excited energy

levels, whereas the idler couples with the ground state of the embedded quasiresonant centers that provide a resonantly enhanced, FWM response. The options in which no population inversion and Raman-like amplification of the signal is involved as well as the one in which OPA can be supported by such incoherent amplification are discussed and compared with the technique proposed earlier,[14,16,17] in which OPA is accompanied by incoherent amplification of the idler. Here, all local optical characteristics including the nonlinear susceptibility exhibit a strong dependence on the intensity for the driving fields and on the frequency resonance offsets of the coupled waves. Hence, the output signal can be tailored through the means of quantum control. It is shown that the indicated changes in the coupling scheme bring about major changes in the properties of the laser-induced transparency of the doped NIM slabs. The possibility of eliminating the detrimental role of the phase mismatch on the tailored transparency of the slab in this case is also shown. Section 5 summarizes the main results, which prove the feasibility of all-optically tailored transparency and amplification in plasmonic NIMs, as well as the creation of a microscopic, mirrorless, backward-wave, optical parametric oscillator that generates contradirected beams of entangled right- and left-handed photons.

2. BASIC PRINCIPLES OF COHERENT NONLINEAR-OPTICAL ENERGY TRANSFER BETWEEN ORDINARY AND BACKWARD-TRAVELING ELECTROMAGNETIC WAVES

The basic idea of compensating losses by coherent energy transfer from control field(s) to the signal field through parametric interaction is illustrated in Fig. 1. We consider traveling electromagnetic waves of the form

$$\mathbf{E}_j(\mathbf{r},t) = (1/2)\mathbf{E}_{0j}\exp[i(\mathbf{k}_j\cdot\mathbf{r}-\omega_j t)] + c.c. \tag{1}$$

Usually, a metamaterial possess NI properties within a certain frequency range and PI properties outside such a domain. We assume the wave at ω_1 with a wave-vector $\mathbf{k}_1$ directed along the z-axis is a negative-phase signal ($n_1 < 0$). Therefore, it is a backward wave (BW) because its energy flow $\mathbf{S}_1 = (c/4\pi)[\mathbf{E_1}\times\mathbf{H_1}]$ appears directed against the z-axis. In the TWM case, shown in Fig. 1(a), a slab of thickness L is illuminated by a higher-

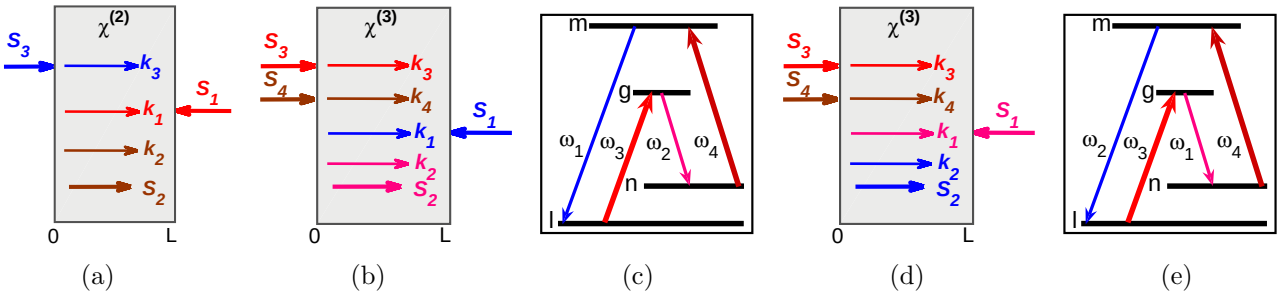

Figure 1. Coupling geometry for three-wave mixing, (a), and four-wave mixing of an ordinary and a backward electromagnetic wave, (b) and (d), and scheme of quantum-controlled four-wave mixing in embedded resonant nonlinear-optical centers, (c) and (e). Here, $\mathbf{S}_1$, $\mathbf{k}_1$ and ω_1 are the energy flow, wave-vector and frequency of the negative-index signal ($n_1 < 1$); $\mathbf{S}_{3,4}$, $\mathbf{k}_{3,4}$ and $\omega_{3,4}$ are those of the positive-index control fields; and $\mathbf{k}_2$ and ω_2 stand for the positive-index idler. (b) and (c) – shortest-wavelength negative-phase signal; depending on the partial relaxation rates, parametric amplification may be assisted by the idler's population-inversion or Raman-type amplification. (d) and (e) – longer-wavelength negative-phase signal; depending on the partial relaxation rates, parametric amplification may be assisted by the signal incoherent amplification attributed to population-inversion or Raman-type gain.

frequency, ordinary, PI wave at ω_3 traveling along the z-axis ($n_3 > 0$). In the FWM case, Fig. 1 (b) and (d), the slab is illuminated by two PI control (pump) waves at ω_3 and ω_4. In both cases, all wave-vectors are co-directed along the the z-axis. Due to parametric interaction, the control and signal fields generate a difference-frequency idler at $\omega_2 = \omega_3 - \omega_1$ (TWM) or at $\omega_2 = \omega_4 + \omega_3 - \omega_1$ (FWM), which is also assumed to be a PI wave ($n_2 > 0$). The idler contributes back into the wave at ω_1 through the same type of the parametric interaction and thus enables OPA at ω_1 by converting the energy of the control fields into the signal. Thus, all of the coupled waves have their wave-vectors co-directed along z, whereas the energy flow of the signal wave, $\mathbf{S}_1$, is counter-directed to

the energy flows of all the other waves, whose wave-vectors are co-directed with their energy flows. Such coupling schemes are in contrast both with the conventional phase-matching scheme for OPA in ordinary materials, where all energy-flows and phase velocities are co-directed, as well as with the early proposal and recent realization of TWM backward-wave mirrorless OPO,[27–29, 31] where both the energy flow and wave-vector of one of the waves are opposite to all others. For the electric quadratic nonlinearity, nonlinear polarizations are sought in the form

$$P_1^{NL} = \chi^{(2)} E_3 E_2^* \exp\{i[(k_3 - k_2)z - \omega_1 t]\}, \quad P_2^{NL} = \chi^{(2)} E_3 E_1^* \exp\{i[(k_3 - k_1)z - \omega_2 t]\}, \tag{2}$$

where $\omega_2 = \omega_3 - \omega_1$ and $k_j = |n_j|\omega_j/c > 0$. Nonlinear FWM polarizations are sought in the form

$$P_1^{NL} = \chi^{(3)} E_3 E_4 E_2^* \exp\{i[(k_3 + k_4 - k_2)z - \omega_1 t]\}, \quad P_2^{NL} = \chi^{(3)} E_3 E_4 E_1^* \exp\{i[(k_3 + k_4 - k_1)z - \omega_2 t]\}, \tag{3}$$

where $\omega_2 = \omega_3 + \omega_4 - \omega_1$ and $k_j = |n_j|\omega_j/c > 0$. We introduce effective amplitudes, a_j, and nonlinear coupling parameters, g_j, which for the quadratic nonlinearity are defined as

$$a_j = \sqrt{|\epsilon_j/k_j|}E_j, \quad g_j = \sqrt{|k_1 k_2/\epsilon_1\epsilon_2|}2\pi\chi_{ej}^{(2)} E_3, \quad g_1 = g_2; \tag{4}$$

and for FWM as

$$a_j = \sqrt{|\epsilon_j/k_j|}E_j, \quad g_j = \sqrt{|k_1 k_2/\epsilon_1\epsilon_2|}2\pi\chi_j^{(3)} E_3 E_4. \tag{5}$$

The quantities $|a_j|^2$ are proportional to the photon numbers in the energy fluxes. Equations for amplitudes a_j are identical for all of the types of nonlinearities studied here:

$$da_1/dz = -g_1 a_2^* \exp(i\Delta k z) + (\alpha_1/2)a_1, \quad da_2/dz = g_2 a_1^* \exp(i\Delta k z) - (\alpha_2/2)a_2. \tag{6}$$

Here, $\Delta k = k_3 - k_2 - k_1$ for TWM, and $\Delta k = k_4 + k_3 - k_2 - k_1$ for FWM. We note the following three fundamental differences in equations (6) as compared with their counterpart in ordinary, PI materials. First, the signs with g_1 are opposite to that with g_2. This is because $\epsilon_1 < 0$ and $\mu_1 < 0$. Second, the opposite sign appears with α_1 because the energy flow $\mathbf{S_1}$ is against the z-axis. Third, the boundary conditions for the signal are defined at the opposite side of the sample as compared to the idler because the energy flows $\mathbf{S_1}$ and $\mathbf{S_2}$ are counter-directed. These modifications lead to dramatic changes in the equation solution as compared with the exponential dependence on z that is characteristic for the ordinary, naturally occurring, PI materials. At $a_{20} = 0$, the equations for the energy distribution for the backward wave, $T_1(z) = |a_1(z)/a_{1L}|^2$, and for the PI idler, $\eta_2(z) = |a_2(z)/a_{1L}^*|^2$, across the slab of thickness L take the form

$$T_1(z) = \left|[\kappa_2 \exp(\beta_1 z) - \kappa_1 \exp(\beta_2 z)]/D\right|^2, \quad \eta_2(z) = \left|[\exp(\beta_1 z) - \exp(\beta_2 z)]/D\right|^2, \tag{7}$$

where

$$\beta_{1,2} = (\alpha_1 - \alpha_2)/4 \pm iR, \quad \kappa_{1,2} = [\pm R + is]/g, \quad R = \sqrt{g^2 - s^2}, \quad g^2 = g_2^* g_1, \quad s = (\alpha_1 + \alpha_2)/4 - i\Delta k/2, \tag{8}$$

$$A_1 = \{a_{1L}\kappa_2 - a_{20}^* \exp[(\beta_2 + i\frac{\Delta k}{2})L]\}/D, \quad A_2 = -\{a_{1L}\kappa_1 - a_{20}^* \exp[(\beta_1 + i\frac{\Delta k}{2})L]\}/D, \tag{9}$$

$$D = \kappa_2 \exp[(\beta_1 + i\frac{\Delta k}{2})L] - \kappa_1 \exp[(\beta_2 + i\frac{\Delta k}{2})L]. \tag{10}$$

Then, the transmission factor for the backward-wave signal at $z = 0$, T_{10}, and the output idler at $z = L$, η_{2L}, are given by

$$T_{10} = \left|\frac{a_1(0)}{a_{1L}}\right|^2 = \left|\frac{\exp\{-[(\alpha_1/2) - s]\,L\}}{\cos RL + (s/R)\sin RL}\right|^2, \quad \eta_{2L} = \left|\frac{a_2(L)}{a_{1L}}\right|^2 = \left|\frac{(g/R)\sin RL}{\cos RL + (s/R)\sin RL}\right|^2. \tag{11}$$

At $a_{1L} = 0$, $a_2(z = 0) = a_{20}$, the slab serves as a *NLO mirror* with a reflectivity (conversion efficiency from ω_2 to ω_1) given by an equation identical to Eq.(11):

$$\eta_{10} = \left|\frac{a_1(0)}{a_{20}^*}\right|^2 = \left|\frac{(g/R)\sin RL}{\cos RL + (s/R)\sin RL}\right|^2. \tag{12}$$

The fundamental difference between the spatial distribution of the signal in ordinary and NI slabs is most explicitly seen at $\alpha_j = \Delta k = 0$. There, the equation for transparency reduces to

$$T_{10} = 1/[\cos(gL)]^2. \tag{13}$$

Equations (11)-(13) show that the output signal and idler experience a sequence of geometrical resonances at $gL \to (2j+1)\pi/2$, (j=0, 1, 2, ...), as functions of the slab thickness L and of the intensity of the control field (factor g). Such behavior is in drastic contrast with that in an ordinary medium, where the signal would grow exponentially as $T_1 \propto \exp(2gL)$. The resonances indicate that strong absorption of the left-handed, negative-phase wave and of the idler can be turned into transparency, amplification and even into *cavity-free self-oscillation* when the denominator tends to zero. The conversion factors η_{10} and η_{2L} experience a similar resonance increase. Self-oscillation would provide for the generation of entangled, counter-propagating, left-handed, $\hbar\omega_1$, and right-handed, $\hbar\omega_2$, photons without a cavity. A similar behavior is characteristic for distributed-feedback lasers and is equivalent to a great extension of the NLO coupling length. It is known that even weak amplification per unit length may lead to lasing provided that the corresponding frequency coincides with high-quality cavity or feedback resonances. Absorption and phase-mismatch may essentially change the properties of the spatial distribution of the fields. Below, we present an investigation of such properties and of the output resonances.

3. EFFECT OF IDLER ABSORPTION AND PHASE-MISMATCH ON ENERGY DISTRIBUTION ACROSS THE NIM SLAB AND ON THE INDUCED TRANSPARENCY

In order to demonstrate the major effects of the idler absorption and phase mismatch on the laser-induced transparency resonances, we consider the model where the dependence of the local linear optical and NLO parameters on the field frequencies and on the intensity of the control field can be neglected and the parameter g is real. Such a model is relevant to, e.g., off-resonant quadratic and cubic nonlinearities attributed to the structural elements of metal-dielectric nanocomposites.[6] The results will be used in the next section for optimization of the transparency achievable through embedded resonant FWM centers with power-dependent local optical parameters. A crucial importance of the outlined geometrical resonances is illustrated in Figs. 2 and 3. Besides the factor g, the local NLO energy-conversion rate for the signal is proportional to the amplitude of the idler (and vice versa) and depends on the phase mismatch Δk. Hence, the fact that the waves decay in opposite directions causes a specific, strong dependence of the entire propagation process and, consequently, of the transmission properties of the slab on the ratio of the signal and the idler decay rates.[15] A typical NIM slab absorbs about 90% of light at the frequencies that are in the NI frequency range. Such absorption corresponds to $\alpha_1 L \approx 2.3$. Since the idler grows toward the back facet of the slab and the signal experiences absorption in the opposite direction, the maximum of the signal for the given parameters may be located inside the slab and its minimum may appear close to the output facet at z=0, which reduces the overall slab transparency. A change in the slab thickness, the intensity of the control fields, or the phase mismatch leads to significant changes in the distributions of the signal and idler along the slab and in their output values (Fig. 2 and 3). Such extraordinary resonance

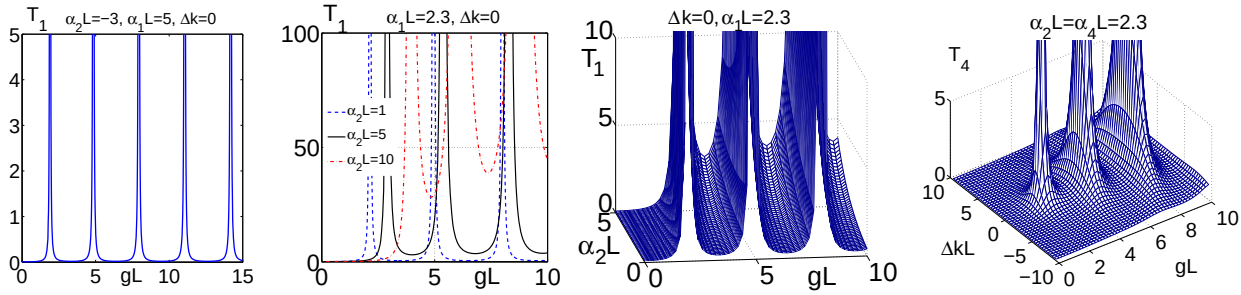

(a) (b) (c) (d)

Figure 2. Effect of idler gain (a), absorption (b) and (c), and phase mismatch (d) on the properties of the transmission resonances for the negative-phase signal.

behavior, which occurs due to the backwardness of the light waves in NIMs, is explicitly seen when compared with similar distributions in ordinary, PI materials depicted in Fig. 3(a). Basically, such induced transparency

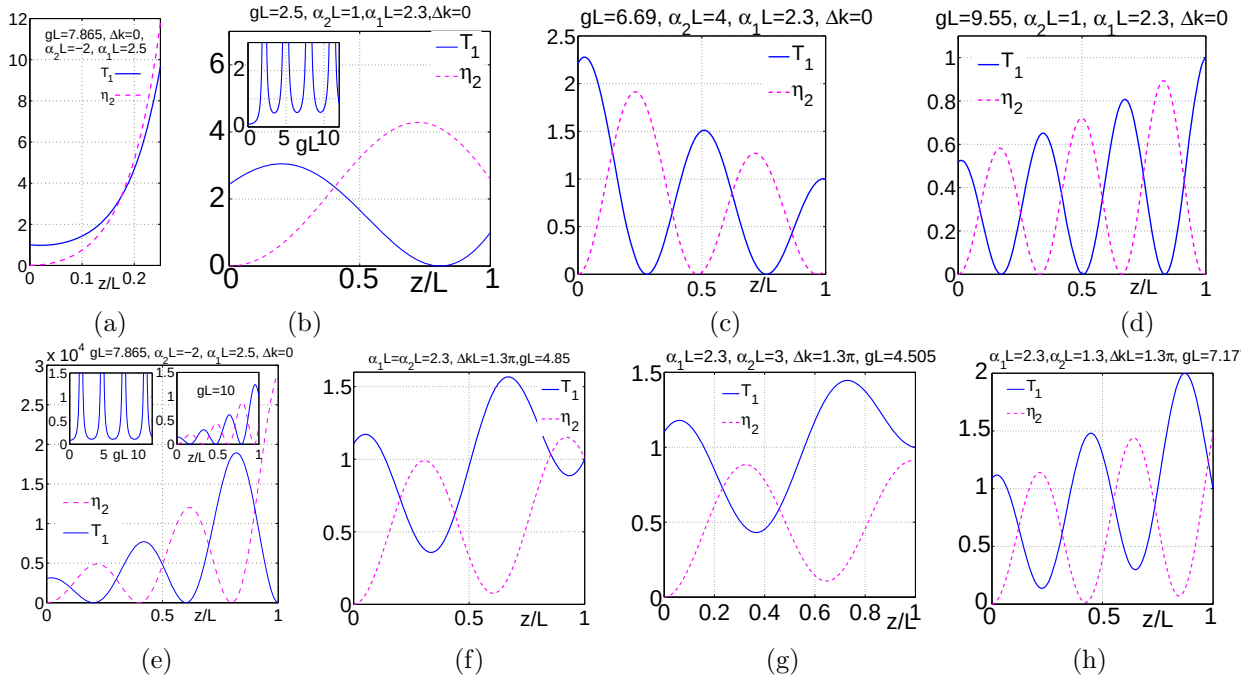

Figure 3. Effect of different signal and idler absorption rates, phase mismatch and intensity of the control fields on the distribution across the slab and on the output values of the signal and the idler. (a) – spatial dependence of the signal and the idler in an ordinary, PI slab.

resonances are narrow, like those depicted in Fig. 2(a) and by the plot corresponding to $\alpha_2 L = 1$ in Fig. 2(b), and the sample remains opaque anywhere beyond the resonance field and the parameters of the sample. If nonlinear susceptibility varies within the negative-index frequency domain, this translates into relatively narrow-band filtering. The slab would become transparent within the broad range of the slab thickness and the control field intensity if the transmission in all of the minimums is about or more than 1. Figures 2(b) and (c) show the feasibility of achieving robust transparency and amplification in a NIM slab at the signal frequency through a wide range of control-field intensities and slab thicknesses by the appropriate adjustment of the absorption indices $\alpha_2 \geq \alpha_1$. Figure 2(b) and (c) depict transmission properties of the NIM slab at $\alpha_1 L = 2.3$ and different magnitudes of the absorption index $\alpha_2 > 0$ that are less than, equal to and greater than α_1. The figures show dramatic changes in the transmission properties with changes in the ratio of the absorption indices for the signal, α_1, and the idler, α_2. It is seen that the transmission does not drop below 1 at $\alpha_2 > \alpha_1$. Hence, larger absorption for the idler is advantageous for robust transmission of the signal, which is counterintuitive. The increase of idler absorption is followed by the relatively small shift of the resonances to larger magnitudes of gL. Oscillation amplitudes grow sharply near the resonances, which indicates *cavity-less self-oscillation*. The distribution of the signal and the idler inside the slab would also dramatically change, as depicted in Fig. 3(b)-(h). These simulations prove that, unless optimized, the signal maximum inside the slab may appear much greater than its output value at $z = 0$. Phase-matching of the positive- and negative-index waves also presents a technical challenge. Figure 2(d) shows the possibility to significantly diminish the negative role of the phase mismatch on the tailored transparency of the slab at the expense of a modest increase of the amplitude of the control field. In this case, the spatial distribution of the signal and the idler may experience a dramatic change with changes in the control field intensities and in the ratio of the absorption indices [Fig. 3(b)-(e)], which also depends on the phase mismatch [Fig. 3(f)-(h)]. As outlined, such dependencies are in strong contrast with their counterparts in PI materials [Fig. 3(a)] and are determined by the backwardness of the coupled waves that is inherent to NIMs.

Only rough estimations can be made regarding $\chi^{(2)}$ attributed to metal-dielectric nanostructures. Assuming

$\chi^{(2)} \sim 10^{-6}$ ESU ($\sim 10^3$pm/V), which is on the order of that for $CdGeAs_2$ crystals, and a control field of $I \sim 100$ kW focused on a spot of $D \sim 50\mu$m in diameter, one can estimate that the typical threshold value of $gL \sim 1$ can be achieved for a slab thickness in the microscopic range of $L \sim 1\mu$m, which is comparable with that of the multilayer NIM samples fabricated to date.[2,4]

4. INDEPENDENT ENGINEERING OF NLO RESPONSE, QUASI-RESONANT FOUR-WAVE MIXING OF ORDINARY AND BACKWARD WAVES AND QUANTUM CONTROL OF TRANSPARENCY OF NIM SLABS

Herein, we describe the feasibility of independently engineering the NI and the resonantly enhanced FWM response of a composite metamaterial with embedded NLO centers. We investigate quasi-resonant FWM and the accompanying processes that allow for coherent energy transfer from the control fields to the counter-propagating NI signal and PI idler. We show that despite introducing additional strong absorption associated with the embedded centers, this opens up opportunities for compensating optical losses in NIMs and for the creation of unique NIM-based photonic microdevices, which are of critical importance for the further development of nanophotonics in NIMs (for a review, see, for example,[1]). Among the specific features considered here is the fact that the nonlinear susceptibility becomes complex in the vicinity of the introduced resonances, which is followed by a phase shift between the fields and the polarizations. We also consider the possibility of quantum control over the overall nonlinear propagation process. Possible schemes of resonant coupling are shown in Figs. 1(c) and (e). Due to the different contributions of populations of coupled energy levels to $\chi_1^{(3)}$ and to $\chi_2^{(3)}$, the latter become different and intensity-dependent.[32] The ratio of real and imaginary parts of $\chi_j^{(3)}$ varies with the change of the resonance offsets. It is also different for schemes depicted in Figs. 1(c) and (e). Figure 4 proves that the detrimental role of even large phase-mismatch can be eliminated through appropriate adjustment of the real and imaginary parts of $\chi_j^{(3)}$. Such a possibility is not available for off-resonant wave mixing.

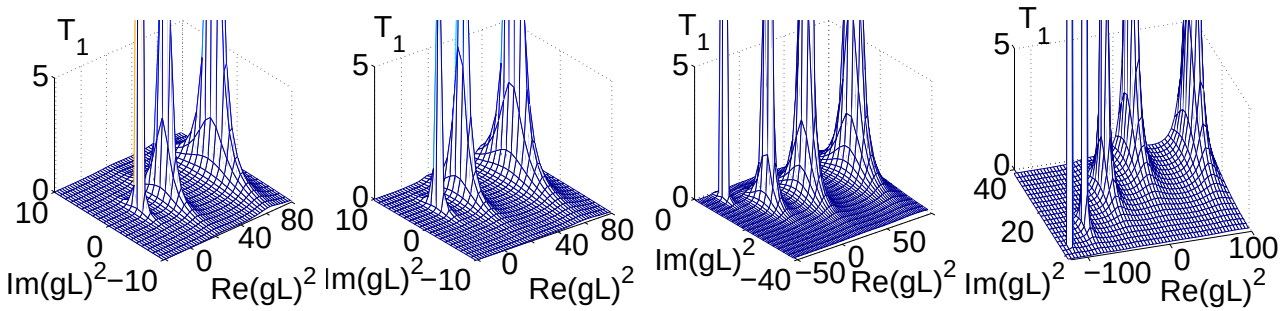

Figure 4. Transmittance T_1 of the NIM slab vs Re(gL) and Im(gL) at different values of linear phase mismatch, Δk. $\alpha_2 L = -2$, $\alpha_1 L = 2.5$. (a): $\Delta k = 0$, (b): $\Delta k L = -\pi$, (c): $\Delta k L = 4\pi$, (d): $\Delta k L = -7\pi$.

As shown in Section 3, coherent energy transfer from control fields to the negative-phase signal depends strongly on the ratio of the absorption rates and on the NLO susceptibilities for the signal and the idler. Figures 1(c) and (e) present two alternative options for quantum control of NLO propagation processes. Figure 1(c) depicts the scheme which offers the possibility of incoherent amplification (population inversion or Raman-type) for the idler.[14,16,17] This possibility depends on the set of quantum relaxation rates inherent to the specific doping agent. Figure 1(e) presents a scheme which offers an alternative possibility. Here, the idler frequency is close to a higher-frequency transition from the ground state, and the signal corresponds to a lower-frequency transition between the excited states. Hence, absorption for the idler is typically larger than for the signal. As shown in Section 3, this situation is advantageous for robust transparency tailoring. No incoherent amplification is possible here for the idler, whereas incoherent absorption for the signal can be controlled and turned to amplification. Such a possibility is also contingent on the appropriate partial population and coherence relaxation rates attributed to the embedded centers. In all of the schemes outlined above, the linear and nonlinear local

parameters can be tailored through quantum control by varying the intensities and frequency-resonance offsets for combinations of the two control driving fields.

First, we consider a numerical model relevant to the coupling scheme depicted in Fig. 1(e) that offers neither the possibility of population inversion nor Raman-type amplification. The fact that all involved optical transitions are absorptive determines the essentially different features of the overall resonant loss-compensation technique compared to that proposed in ref.[14,16,17] The following model, which is characteristic of ions and some molecules embedded in a solid host, has been adopted: energy level relaxation rates $\Gamma_n = 20$, $\Gamma_g = \Gamma_m = 120$ (all in 10^6 s^{-1}); partial transition probabilities $\gamma_{gn} = 50$, $\gamma_{mn} = 90$, (all in 10^6 s^{-1}); homogeneous transition half-widths Γ_{gl}=1.8, Γ_{mn}=1.9, Γ_{gn}=1, Γ_{ml}=1.5, $\Gamma_{mg} = 5\times10^{-2}$, $\Gamma_{nl} = 5\times10^{-3}$ (all in 10^{11} s^{-1}); $\lambda_1 = 756$ nm and $\lambda_2 = 480$ nm. The density-matrix method[32] is used for calculating the intensity-dependent local parameters while accounting for the quantum nonlinear interference effects. This allows us to investigate the changes in absorption, amplification, and refractive indices as well as in the magnitudes and signs of the NLO susceptibilities caused by the control fields. These changes depend on the population redistribution over the coupled levels, which in turn strongly depends on the ratio of the partial transition probabilities. The results of numerical simulations are summarized in Fig. 5. Here, $\Omega_1 = \omega_1 - \omega_{gn}$; other resonance detunings Ω_j are defined in a similar way. Coupling Rabi

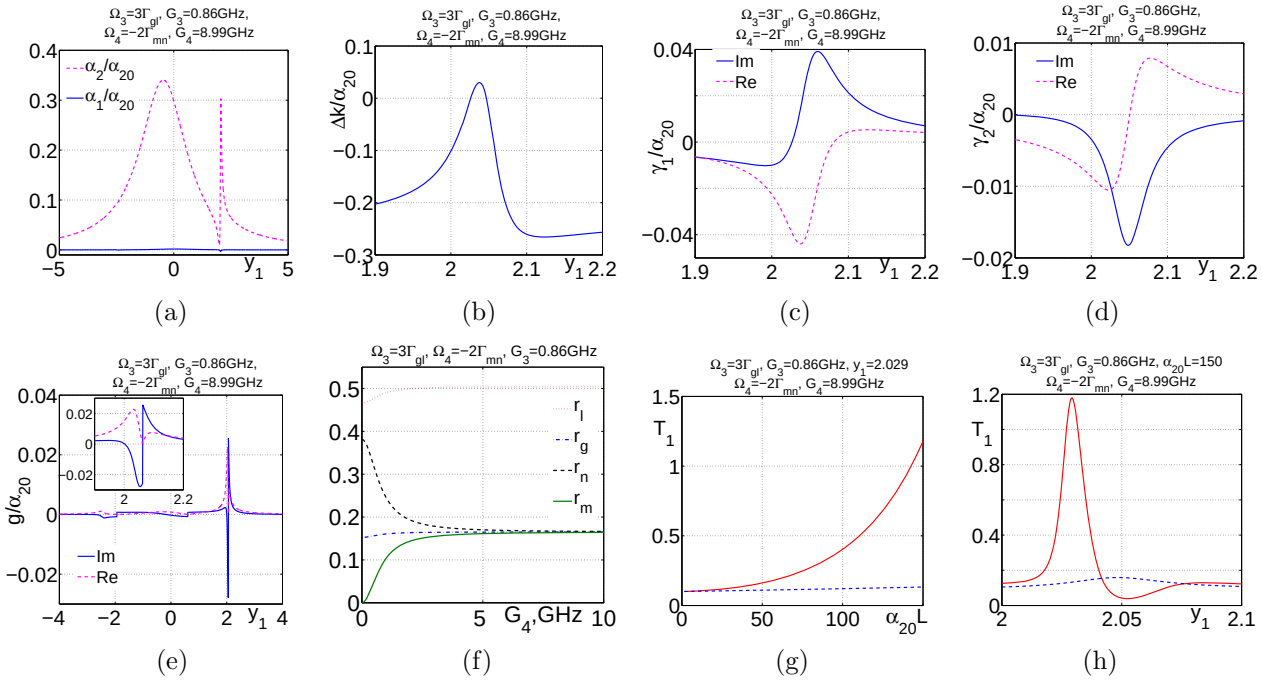

Figure 5. Quasi-resonant coupling, Fig. 1(e), at quantum relaxation rates which make population inversion at any transition and Raman-type gain impossible for both the idler and the signal. $y_1 = (\omega_1 - \omega_{gn})/\Gamma_{gn}$, $\omega_2 = \omega_3 + \omega_4 - \omega_1$. (a): absorption indices for the signal and the idler; (b): phase mismatch; (c)-(e): four-wave mixing coupling parameters; (f): energy level populations; (g) and (h): transmission factor, the dashed line shows transmission at $\chi^{(3)} = 0$. Coupling Rabi frequencies and resonance frequency offsets for the control fields are: G_3=0.86 GHz, $\Omega_3 = 3\Gamma_{gl}$; G_4=8.99 GHz, $\Omega_4 = -2\Gamma_{mn}$.

frequencies are introduced as $G_3 = E_3 d_{lg}/2\hbar$ and $G_4 = E_4 d_{nm}/2\hbar$. The quantity α_{20} denotes the fully resonant value of absorption introduced by the embedded centers at $\omega_2 = \omega_{ml}$ with all driving fields turned off. Figure 5(a) displays the modified absorption indices attributed to the embedded centers. It shows no gain for the signal and the idler. The narrow spectral structure in the wing of the absorption spectrum for the idler is attributed to quantum nonlinear interference effects[32] caused by the modulation of the probability amplitudes, which exhibits itself as an effective splitting of the energy levels coupled with the driving fields. The width of the structure and of the frequency band for the most effective FWM, Fig. 5(c)-(e), are determined by the lowest coherence relaxation rate at transition nl. Figure 5(b) shows the contribution to the phase mismatch in the vicinity of this structure. Figures 5(c) and (d) indicate that the real and imaginary parts of the NLO susceptibilities

become commensurate for the given susceptibility, but differ by sign and are several times different in magnitude than their counterparts for the idler. This occurs due to the fact that various population differences contribute in different ways to the NLO susceptibilities,[32] and driving fields cause significant redistributions of the level populations [Fig. 5(f)]. At the Rabi frequencies and frequency offsets for the driving control fields indicated in Fig. 5, the relative energy-level populations are: $r_l \approx 0.504$, $r_g \approx 0.165$, $r_n \approx 0.167$, $r_m \approx 0.164$. The losses in the host NIM are accounted for and taken to be fixed and equal to $\alpha_{NIM1}L = 2.3$ for the signal and $\alpha_{NIM2}L = 2.1$ for the idler. Figure 5(g) shows transmission at $y_1 = 2.029$ and $\alpha_{20}L < 150$, which appears at the left side of the first geometrical resonance shown in Fig. 3. Figure 5(h) depicts spectral properties of the transmission at $\alpha_{20}L = 150$ with other parameters fixed. Dashed lines in Figs. 5(g) and (h) present transmission at $\chi^{(3)}$=0, which proves that the induced transparency is due to coherent energy transfer from the control fields to the signal through FWM.

For the above-indicated characteristics of the involved optical transitions, the magnitude G=1 GHz corresponds to control field intensities on the order of of $I \sim 1$ W/(0.1mm)^2. Assuming a resonance absorption cross-section $\sigma_{40} \sim 10^{-16}$ cm^2, which is typical for transitions with oscillator strength of about one, and a concentration of embedded centers $N \sim 10^{19}$ cm^{-3}, we obtain $\alpha_{20} \sim 10^3$ cm^{-1} and a required slab thickness in the microscopic range $L \sim 100$ μm. The contribution to the index of refraction by the impurities is estimated as $\Delta n < 0.5(\lambda/4\pi)\alpha_{40} \sim 10^{-3}$, which essentially does not change the negative refractive index.

For comparison, consider the same coupling scheme depicted in Fig. 1(e) but with an alternative model that allows for population inversion and Raman-type gain for the signal: $\Gamma_n = 20$, $\Gamma_g = \Gamma_m = 120$ (all in 10^6 s^{-1}); partial transition probabilities $\gamma_{gn} = 4$, $\gamma_{mn} = 5$, (all in 10^6 s^{-1}); homogeneous transition half-widths Γ_{gl}=1, Γ_{mn}=1.8, Γ_{gn}=1.5, Γ_{ml}=1.9, $\Gamma_{mg} = 5 \times 10^{-2}$, $\Gamma_{nl} = 1 \times 10^{-3}$ (all in 10^{12} s^{-1}); $\lambda_1 = 756$ nm and $\lambda_2 = 480$ nm. The results of numerical experiments with these parameters are summarized in Fig. 6.

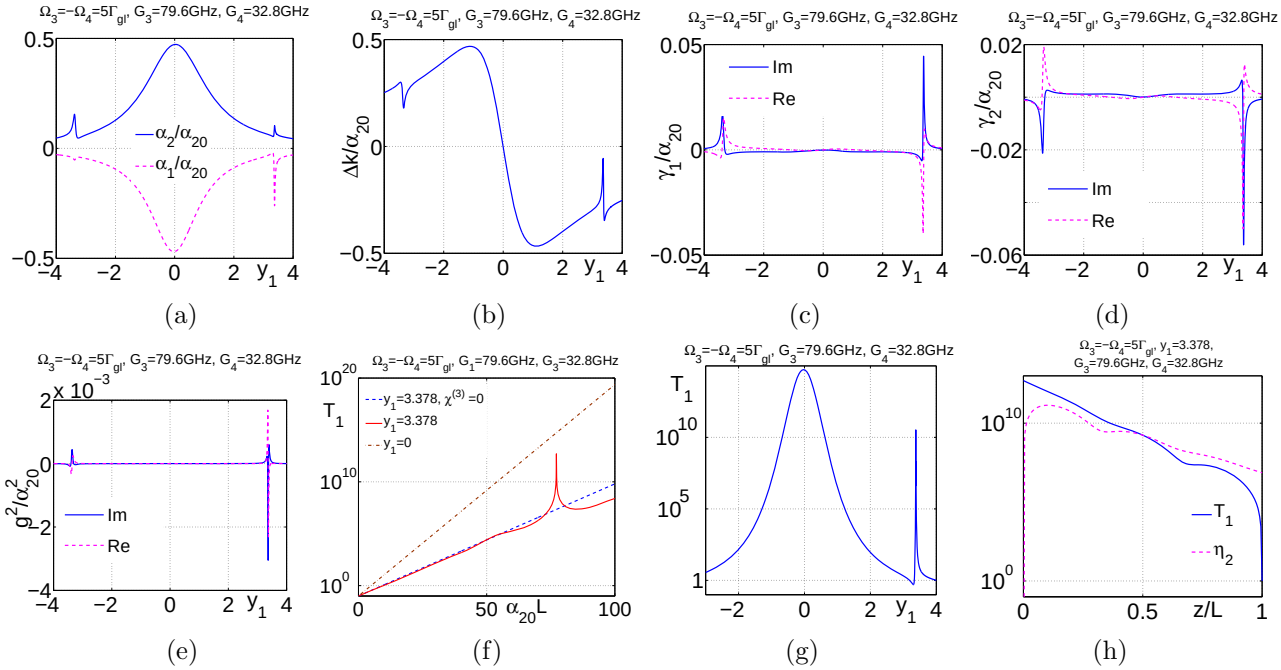

Figure 6. Quasi-resonant coupling, Fig. 1(e), at quantum relaxation rates which make possible population inversion at the signal transition gn and Raman-type gain for the signal. $y_1 = (\omega_1 - \omega_{gn})/\Gamma_{gn}$, $\omega_2 = \omega_3 + \omega_4 - \omega_1$. (a): absorption index for the idler and amplification index for the signal; (b): phase mismatch; (c)-(e): four-wave mixing coupling parameters; (f) and (g): transmission factor, dashed lines in panel (f) show transmission at $\chi^{(3)} = 0$; (h): distribution of the signal and the idler across the slab. Coupling Rabi frequencies and resonance frequency offsets for the control fields are: G_3=79.6 GHz, G_4=32.8 GHz, $\Omega_3 = -\Omega_4 = 5\Gamma_{gl}$.

At the selected coupling Rabi frequencies G_3=79.6 GHz, G_4=32.8 GHz and resonance offsets $\Omega_3 = -\Omega_4 = 5\,\Gamma_{gl}$

the relative populations of the energy levels are $r_l \approx 0.49$, $r_g \approx 0.48$, $r_n \approx 0.016$, $r_m \approx 0.014$, which indicates population inversion at the signal transition gn. Figure 6(a) displays absorption for the idler and gain for the signal. The narrow spectral structures in the wing of the amplification index for the signal are associated with quantum nonlinear interference effects[32] that at large detunings of the control field E_3 convert into Raman gain. Figure 6(b) shows the contribution to the phase mismatch that are attributed to the embedded resonant centers driven by the control fields. Figures 6(c)-(e) depict FWM coupling parameters also modified by the driving control fields. The plots indicate that the strongest FWM coupling occurs in the vicinity of the signal frequency offset $y_1 = 3,378$ that corresponds to quasi-Raman gain in the wing of the population inversion gain. Figure 6(f) shows transmission in the center of the gn transition and at $y_1 = 3,378$. Like in the previous model, the losses in the host NIM material are accounted for and taken to be fixed and equal to $\alpha_{NIM1}L = 2.3$ for the signal and $\alpha_{NIM2}L = 2.1$ for the idler. The peak at $\alpha_{20}L = 77.2$ is attributed to OPA superimposed on the background of the Raman gain (dashed line). The other, steeper, straight line shows transmission in the center of the transition, which accounts for both population inversion and parametric gain. However, the dominant contribution here comes from the population inversion. Figure 6(g) shows the spectral properties of the transmission at $\alpha_{20}L = 77.2$. The narrow peak originates from FWM assisted by Raman gain. Figure 6(h) displays the distribution of the signal and the idler at $y_1 = 3,378$ across the slab. The resonance in Fig. 6(f), which is specific for FWM of backward and ordinary traveling waves, provides amplification about five orders stronger than that of the pure Raman gain. This can be used for tailoring the amplification and generation of negative phase signals outside the transition resonance.

5. CONCLUSIONS

The possibility of producing and tailoring a laser-induced optical transparency in a negative-index metamaterial slab through nonlinear-optical coherent energy transfer between ordinary control wave(s) and a negative-phase backward signal is shown and confirmed by numerical simulations. Two possible types of nonlinear-optical responses are considered. One is off-resonant three or four-wave mixing through nonlinear susceptibilities that are assumed to be attributable to the metamaterial nanostructure and are independent of the intensities and frequencies of the control optical fields. The other option is the independent engineering of a resonantly enhanced, four-wave mixing nonlinearity by embedding nonlinear-optical centers in a negative-index host matrix. Here, all local parameters are intensity-dependent and can be tailored by the driving control fields through the means of quantum control. The outcomes are shown to be strongly dependent on the specific scheme of the coupled quantum transitions and their relaxation properties. In the latter case, the proposed specific coupling scheme suggests that the frequency of the negative-phase signal should fall in the vicinity of the transition between the excited levels of the centers, while the idler frequency appears coupled with the absorptive transition from the ground state. Two numerical models with different relaxation parameters are explored and compared. The relaxation properties of the first model make any population inversion or Raman gain impossible in the system. Conversely, four-wave mixing attributed to the second model is always accompanied by population inversion and Raman gain of the signal. The schemes under investigation are different from the previously proposed schemes and exhibit essentially different features. The extraordinary properties of the nonlinear-optical propagation processes in both types of outlined metamaterials are investigated. These properties are in drastic contrast with their counterparts in ordinary, positive-index materials. The focus of this work is on the possibility of compensating the strong losses inherent to metal-dielectric negative-index metamaterials and on producing laser-induced optical transparency and gain for the negative-phase signal. In the case of a frequency- and intensity-independent nonlinear-optical response of the composite, the feasibility of producing transparency and amplification through the entire negative-index frequency domain above a certain control laser field intensity is demonstrated. This is shown to be possible by adjusting the absorption index of the idler to be greater than that for the negative-index signal. Specific features of the quantum control attributed to the outlined numerical models are investigated. It is shown that, despite the additional absorption introduced, these systems allow for transformable optics through quantum switching, filtering and amplification of negative-phase light. In addition, the possibility of realizing a miniature, mirrorless optical parametric generator of entangled, contra-propagating, backward and ordinary waves is also shown and supported by numerical simulations. The extraordinary features predicted in this work stem from the backwardness of electromagnetic waves, which is a feature inherent to this type of metamaterial.

ACKNOWLEDGMENTS

This work was supported by the U. S. Army Research Laboratory and by the U. S. Army Research Office under grants number W911NF-0710261 and 50342-PH-MUR, and by the Siberian Division of the Russian Academy of Sciences under Integration Project No 5.

REFERENCES

1. V. M. Shalaev, "Optical negative-index metamaterials," *Nat. Photonics* **1**, pp. 41–48, Jan. 2007.
2. C. M. Soukoulis and M. Kafesaki, "Weakly and strongly coupled optical metamaterials." Invited talk at the Nanometa 2009, The 2nd European Topical Meeting on Nanophotonics and Metamaterials 5 - 8 January, Seefeld, Tirol, Austria, 2009.
3. N. Katsarakis, G. Konstantinidis, A. Kostopoulos, R. S. Penciu, T. F. Gundogdu, M. Kafesaki, E. N. Economou, T. Koschny, and C. M. Soukoulis, "Magnetic response of split-ring resonators in the far-infrared frequency regime," *Opt. Lett.* **30**(11), pp. 1348–1350, 2005.
4. X. Zhang, "Optical bulk metamaterials." Plenary talk at the Nanometa 2009, The 2nd European Topical Meeting on Nanophotonics and Metamaterials 5 - 8 January, Seefeld, Tirol, Austria, 2009.
5. J. Valentine, S. Zhang, T. Zentgraf, E. Ulin-Avila, D. A. Genov, G. Bartal, and X. Zhang, "Three-dimensional optical metamaterial with a negative refractive index ," *Nature* **455**, pp. 376–379, Sept. 2008.
6. M. W. Klein, M. Wegener, N. Feth, and S. Linden, "Experiments on second- and third-harmonic generation from magnetic metamaterials," *Optics Express* **15**, pp. 5238–5247, Apr. 2007.
7. M. W. Klein, M. Wegener, N.-A. Feth, and S. Linden, "Experiments on second- and third-harmonic generation from magnetic metamaterials: erratum," *Opt. Express* **16**(11), pp. 8055–8055, 2008.
8. V. M. Agranovich, Y. R. Shen, R. H. Baughman, and A. A. Zakhidov, "Linear and nonlinear wave propagation in negative refraction metamaterials," *Phys. Rev. B* **69**, p. 165112(7), Apr. 2004.
9. I. V. Shadrivov, A. A. Zharov, and Y. S. Kivshar, "Second-harmonic generation in nonlinear left-handed metamaterials," *J. Opt. Soc. Am. B* **23**(3), pp. 529–534, 2006.
10. A. K. Popov, V. V. Slabko, and V. M. Shalaev, "Second harmonic generation in left-handed metamaterials," *Laser Phys. Lett.* **3**(6), pp. 293–296, 2006.
11. A. K. Popov and V. M. Shalaev, "Negative-index metamaterials: second-harmonic generation, Manley Rowe relations and parametric amplification," *Applied Physics B: Lasers and Optics* **84**, pp. 131–137, July 2006.
12. M. Scalora, G. D'Aguanno, M. Bloemer, M. Centini, D. de Ceglia, N. Mattiucci, and Y. S. Kivshar, "Dynamics of short pulses and phase matched second harmonic generation in negative index materials," *Opt. Express* **14**, pp. 4746–4756, May 2006.
13. A. K. Popov and V. M. Shalaev, "Compensating losses in negative-index metamaterials by optical parametric amplification," *Opt. Lett.* **31**, pp. 2169–2171, July 2006.
14. A. K. Popov, S. A. Myslivets, T. F. George, and V. M. Shalaev, "Four-wave mixing, quantum control, and compensating losses in doped negative-index photonic metamaterials," *Opt. Lett.* **32**, pp. 3044–3046, 2007.
15. A. K. Popov and S. A. Myslivets, "Transformable broad-band transparency and amplification in negative-index films," *Applied Physics Letters* **93**(19), p. 191117(3), 2008.
16. A. K. Popov, S. A. Myslivets, and V. M. Shalaev, "Resonant nonlinear optics of backward waves in negative-index metamaterials," *Applied Physics B: Lasers and Optics* **94**, pp. (on–line Feb. 13), 2009.
17. A. K. Popov, S. A. Myslivets, and V. M. Shalaev, "Microscopic mirrorless negative-index optical parametric oscillator," *Opt. Lett.* **34**(8), pp. 1165–1167, 2009.
18. A. K. Popov, S. A. Myslivets, and V. M. Shalaev, "Coherent nonlinear optics and quantum control in negative-index metamaterials," *to appear in J. Opt. A: Pure Appl. Opt.* **11**, pp. xxx–xxx(13pp.), 2009.
19. N. Lazarides and G. P. Tsironis, "Coupled nonlinear schrödinger field equations for electromagnetic wave propagation in nonlinear left-handed materials," *Phys. Rev. E* **71**, p. 036614, Mar 2005.
20. P. Tassin, L. Gelens, J. Danckaert, I. Veretennicoff, G. V. der Sande, P. Kockaert, and M. Tlidi, "Dissipative structures in left-handed material cavity optics," *Chaos: An Interdisciplinary Journal of Nonlinear Science* **17**(3), p. 037116(11), 2007.

21. P. Kockaert, P. Tassin, G. V. der Sande, I. Veretennicoff, and M. Tlidi, "Negative diffraction pattern dynamics in nonlinear cavities with left-handed materials," *Physical Review A (Atomic, Molecular, and Optical Physics)* **74**(3), p. 033822(8), 2006.
22. A. Boardman, N. King, R. Mitchell-Thomas, V. Malnev, and Y. Rapoport, "Gain control and diffraction-managed solitons in metamaterials," *Metamaterials* **2**(2-3), pp. 145 – 154, 2008. Metamaterials'2007 Congress.
23. G. D'Aguanno, N. Mattiucci, M. Scalora, and M. J. Bloemer, "Bright and dark gap solitons in a negative index fabry-pérot etalon," *Phys. Rev. Lett.* **93**, p. 213902, Nov 2004.
24. N. M. Litchinitser, I. R. Gabitov, A. I. Maimistov, and V. M. Shalaev, "Negative refractive index metamaterials in optics," in *Progress in Optics*, E. Wolf, ed., **51**, pp. 1–68, Elsevier, 2007.
25. N. M. Litchinitser, I. R. Gabitov, A. I. Maimistov, and V. M. Shalaev, "Effect of an optical negative index thin film on optical bistability," *Opt. Lett.* **32**, pp. 151–153, Jan. 2007.
26. A. Maimistov and I. Gabitov, "Nonlinear optical effects in artificial materials," in *Eur. Phys. J. Special Topics "Nonlinear Waves in Complex Systems: Energy Flow and Geometry"*, J.-G. Caputo and M. P. Soerensen, eds., **147**, pp. 265–286, Springer, 2007.
27. S. E. Harris, "Proposed backward wave oscillation in the infrared," *Appl. Phys. Lett.* **9**, pp. 114–116, Aug. 1966.
28. J. B. Khurgin, "Optical parametric oscillator: Mirrorless magic," *Nat. Photonics* **1**, pp. 446–447, Aug. 2007.
29. C. Canalias and V. Pasiskevicius, "Mirrorless optical parametric oscillator," *Nat. Photonics* **1**, pp. 459–462, Aug. 2007.
30. A. Yariv, *Quantum Electronics, 2d ed.*, New York: Wiley, 1975.
31. K. I. Volyak and A. S. Gorshkov, "Investigations of a reverse-wave parametric oscillator," *Radiotekhnika i Elektronika (Radiotechnics and Electronics) [in Russian]* **18**, pp. 2075–2082, 1973.
32. A. K. Popov, S. A. Myslivets, and T. F. George, "Nonlinear interference effects and all-optical switching in optically dense inhomogeneously broadened media," *Phys. Rev. A* **71**, p. 043811(13), Apr. 2005.